PROCEEDINGS OF SPIE

SPIEDigitalLibrary.org/conference-proceedings-of-spie

High-throughput activator sequence selection for silver nanocluster beacons

Yu-An Kuo, Cheulhee Jung, Yu-An Chen, James Rybarski, Trung Nguyen, et al.

Yu-An Kuo, Cheulhee Jung, Yu-An Chen, James R. Rybarski, Trung D. Nguyen, Yin-An Chen, Hung-Che Kuo, Oliver S. Zhao, Victor A. Madrid, Yuan-I Chen, Yen-Liang Liu, John A. Hawkins, Jeffrey T. Petty, Ilya J. Finkelstein, Hsin-Chih Yeh, "High-throughput activator sequence selection for silver nanocluster beacons," Proc. SPIE 10893, Reporters, Markers, Dyes, Nanoparticles, and Molecular Probes for Biomedical Applications XI, 108930G (7 March 2019); doi: 10.1117/12.2510649



Event: SPIE BiOS, 2019, San Francisco, California, United States

High-throughput activator sequence selection for silver NanoCluster Beacons

Yu-An Kuo¹, Cheulhee Jung⁹, Yu-An Chen¹, James R. Rybarski², Trung D. Nguyen¹, Yin-An Chen⁵, Hung-Che Kuo², Oliver S. Zhao¹, Victor A. Madrid⁶, Yuan-I Chen¹, Yen-Liang Liu¹, John A. Hawkins³, Jeffrey T. Petty⁷, Ilya J. Finkelstein^{2, 4, *} and Hsin-Chih Yeh^{1, 8, *}

¹Department of Biomedical Engineering, University of Texas at Austin, Austin, USA
²Department of Molecular Biosciences, University of Texas at Austin, Austin, TX 78712, USA
³Institute for Computational Engineering and Science, University of Texas at Austin, Austin, USA
⁴Center for Systems and Synthetic Biology, University of Texas at Austin, Austin, USA
⁵Department of Chemistry, University of Texas at Austin, Austin, USA
⁶Department of Mechanical Engineering, University of Texas at El Paso, El Paso, USA
⁷Department of Chemistry, Furman University, Greenville, USA
⁸Texas Materials Institute, University of Texas at Austin, Austin, USA
⁹Korea University, Seoul, Republic of Korea

ABSTRACT

Invented in 2010, NanoCluster Beacons (NCBs) (1) are an emerging class of turn-on probes that show unprecedented capabilities in single-nucleotide polymorphism (2) and DNA methylation (3) detection. As the activation colors of NCBs can be tuned by a near-by, guanine-rich activator strand, NCBs are versatile, multicolor probes suitable for multiplexed detection at low cost. Whereas a variety of NCB designs have been explored and reported, further diversification and optimization of NCBs require a full scan of the ligand composition space. However, the current methods rely on microarray and multi-well plate selection, which only screen tens to hundreds of activator sequences (4, 5). Here we take advantage of the next-generation-sequencing (NGS) platform for high-throughput, large-scale selection of activator strands. We first generated a ~10⁴ activator sequence library on the Illumina *MiSeq* chip. Hybridizing this activator sequence library with a common nucleation sequence (which carried a nonfluorescent silver cluster) resulted in hundreds of *MiSeq* chip images with millions of bright spots (i.e. light-up polonies) of various intensities and colors. With a method termed Chip-Hybridized Associated Mapping Platform (CHAMP) (6), we were able to map these bright spots to the original DNA sequencing map, thus recovering the activator sequence behind each bright spot. After assigning an "activation score" to each "light-up polony", we used a computational algorithm to select the best activator strands and validate these strands using the traditional in-solution preparation and fluorometer measurement method. By exploring a vast ligand composition space and observing the corresponding activation behaviors of silver clusters, we aim to elucidate the design rules of NCBs.

Keywords: silver nanoclusters, turn-on probes, next-generation sequencing, fluorescence microscopy, nanobiosensors

1. INTRODUCTION

Activated under specific conditions but otherwise remaining dark, turn-on probes (or activatable probes) have become an important tool in quantitative biology and analytical chemistry as they allow for sensitive detection or imaging of minute amount of targets (7). While turn-on probes eliminate the need to remove unbound probes which greatly simplifies the assay, the development of new turn-on probes are generally constrained by the scarce activation mechanisms (e.g. FRET), the limited activation colors (e.g. existing FRET pairs), and the poor activation ratio (\sim 30-fold for a typical molecular beacon). In addition, turn-on probes are often complicated and costly to make (e.g. >\$500 for a typical molecular beacon). In 2010, a new type of turn-on probes, termed NanoCluster Beacons (NCBs), was introduced, which employ DNA-templated, few-atom silver nanoclusters (\sim 4g₁₀) as the fluorescent reporters (8) (which are brighter and more photostable than typical organic dyes) and a newly discovered guanine-proximity-induced fluorescence enhancement phenomenon as the activation mechanism (1). Compared to other turn-on probes, NCBs are low cost (1/10 of the cost of molecular beacons),

Reporters, Markers, Dyes, Nanoparticles, and Molecular Probes for Biomedical Applications XI, edited by Samuel Achilefu, Ramesh Raghavachari, Proc. of SPIE Vol. 10893, 108930G ⋅ © 2019 SPIE CCC code: 1605-7422/19/\$18 ⋅ doi: 10.1117/12.2510649

easy to prepare (one-step preparation at room temperature), and having as large as 1,500-fold fluorescence enhancement upon activation. Since their first introduction to the field, NCBs have enabled the detection of nucleic acids (2, 9, 10), proteins (11-13), metabolites (14) and cancer cells (15).

A typical NCB consists of a nanocluster-nucleation strand (or NC probe, which carries a dark silver cluster) and a guanine-rich activator strand (or activator probe, Fig. 1A). These two strands bind in juxtaposition to a DNA target, which enables the guanine-rich activator sequence to interact with the dark silver cluster and transform the cluster from a non-emissive state to a highly fluorescent state. Fluorescence thus occurs only when a specific DNA target is present in solution. As the emission spectra of silver nanoclusters are highly sensitive to their coordination nucleobase environments (through short-range interactions that are neither FRET nor electron transfer (16), which we collectively term "ligand effects"), we have previously diversified NCBs by systematically varying the NC probe sequences, the activator probe sequences, and the alignment between the two strands (Fig. 1B) (9). Whereas a complementary palette of NCBs (from green, yellow, red to near-infrared) has been successfully created (16), we are not sure if the published NCBs are the brightest and the most photostable among all possible NCB designs. As the investigation was conducted by mixing one-pair of strands at a time in a test tube and measuring the resulting emission in a fluorometer, less than 100 sequences were screened, which only represented a tiny nucleobase composition space . It is clear that further diversification and optimization of NCBs require a full scan of the ligand composition space.

To screen a vast library of activator sequences and select the best sequences for future NCB designs, we repurpose a next-generation sequencing chip (Illumina *MiSeq*, Fig. 2) to contain 12,288 distinct activator sequences, each having ~250 duplicate clonal DNA clusters on the chip which are also called "polonies". Hybridizing these 12,288 activator sequences on chip with a common NC probe (with carries a nonfluorescent silver cluster) can result in hundreds of *MiSeq* chip images with millions of bright spots (i.e. light-up polonies) of various intensities and colors. With a method termed Chip-Hybridized Associated Mapping Platform (CHAMP)(6), we are able to map these bright spots to the original DNA sequencing map, thus recovering the activator sequence behind each bright spot. After assigning an "activation score" to each "light-up polony", we use a computational algorithm to select the best activator strands and validate these strands using the traditional in-solution preparation and fluorometer measurement method (Fig. 2). By exploring a vast ligand composition space and observing the corresponding activation behaviors of silver clusters, we aim to elucidate the design rules of NCBs.

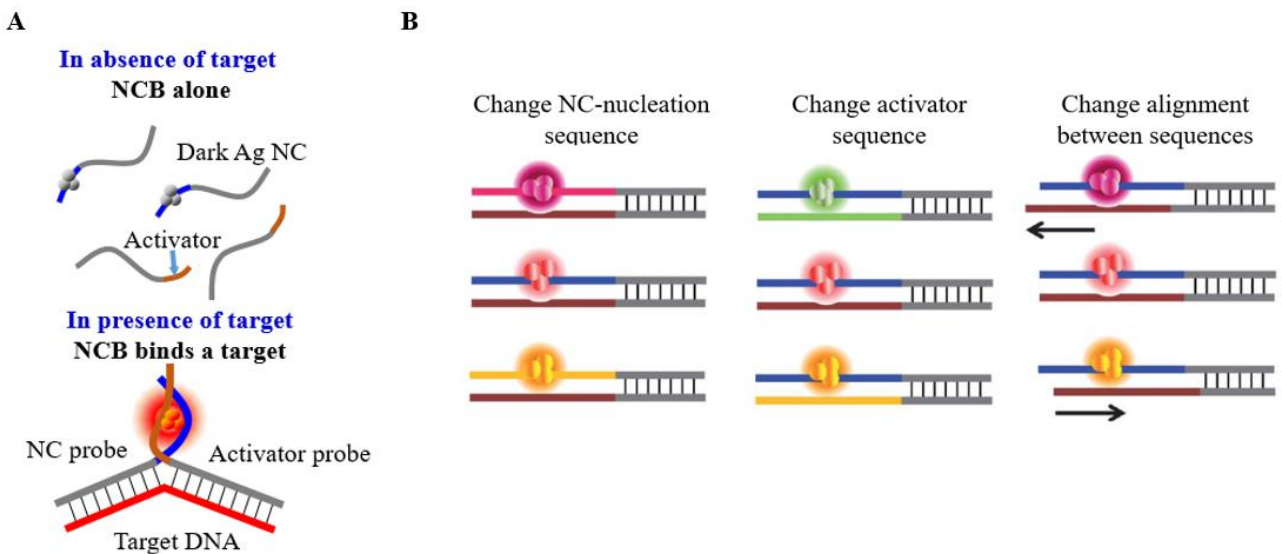


Figure 1. (A) The schematic of the target sequence detection using NCB. Upon hybridization, NC probe, activator probe and target strand form a 3-way junction, bringing the guanine-rich activator sequence to interact with the silver cluster. Such interactions significantly enhance the fluorescence emission of the silver cluster. **(B)** Three different strategies to tune NCB fluorescence. By changing NC-nucleation sequence, activator sequence and alignment between sequences, we can tune the spectra of NCBs from green to near-infrared. In this report, we focus on selecting activator sequences from a vast library. The figure is adapted from reference [9].

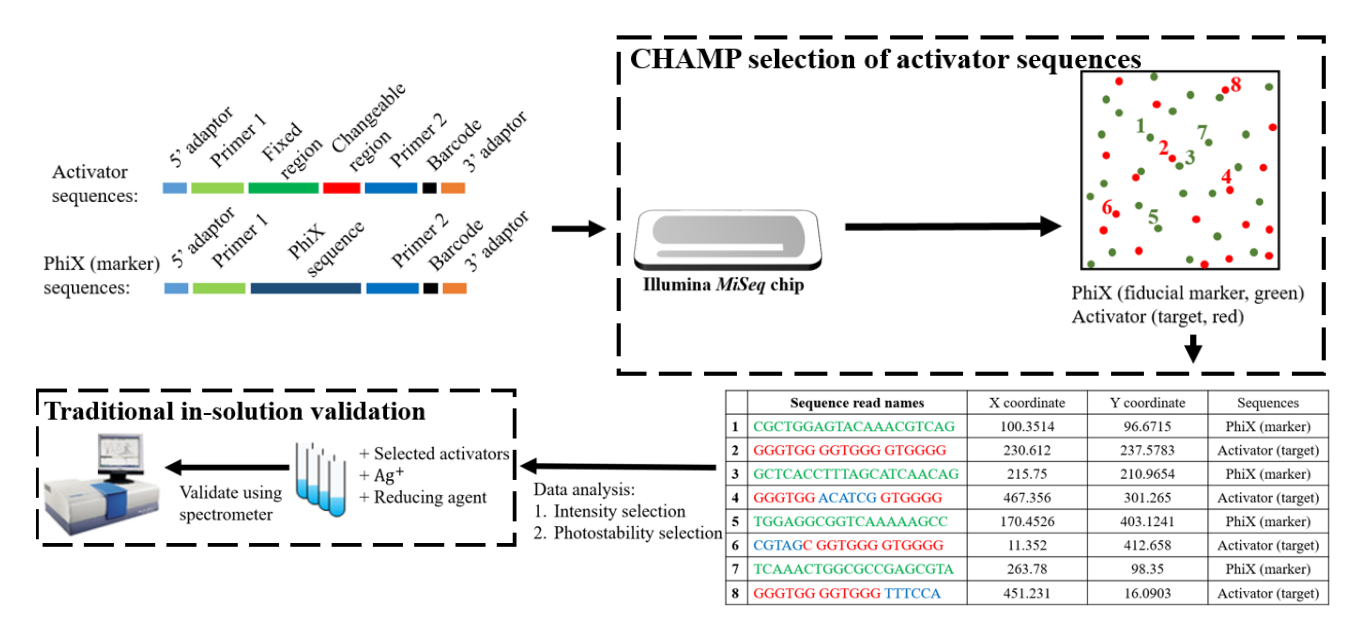


Figure 2. The schematic of CHAMP-NCB selection platform. A library of 12,288 of activator sequences and a group of fiducial marker sequences (PhiX) were first synthesized and transferred to an Illumina *MiSeq* chip. This chip was sequenced at the core facility, generating a sequence map (i.e. a FastQ file). A common NC probe (C55) was then introduced to the chip, hybridizing with the activator sequence library and lighting up each polony. The sequence information of each light-up polony (reads 2, 4, 6 and 8; blue-color sequences) could be extracted by mapping the newly acquired *MiSeq* chip image to the original sequence map, through the alignment of PhiX fiducial markers (reads 1, 3, 5 and 7; green-color sequences). Using this massively parallel, high-throughput analysis platform, we would be able to select NCBs based on their activation brightness and photostability under constant illumination.

2. MATERIALS AND METHODS

2.1 Library preparation and initial *MiSeq* sequencing

2.2 Silver cluster nucleation process on the C55 NC probe

Following the protocol previously reported by us (17), 7.5 μ l 1.2 mM C55 NC probe was added to 562 μ l 20 mM sodium phosphate buffer at pH 6.6. After vortex and centrifugation, 27 μ l 4 mM AgNO₃ was added to the reaction and equilibrated for 10 minutes. Silver ions were reduced by adding 4.2 μ l of freshly prepared 13.25 mM NaBH₄ to the reaction.

The solution was stored in the dark overnight (\sim 18 hours, at room temperature) before purification. The final concentration of the NC probes should be 15 μ M.

2.3 Purification of the C55 NC probes and hybridization of C55 NC probes with activator probes on MiSeq chip

Since the yield for forming functional silver clusters on DNA was not 100%, we purified the NC probe sample by removing the unlabeled (i.e. nonfunctional) NC probes using a spin column (Amicon Ultra-0.5 Centrifugal Filter Devices, catalog number: UFC500324). 150 µl of the NC probe sample was mixed with 350 µl 200 mM sodium phosphate buffer in the filter device and centrifuged at 14,000 RPM for 10 minutes (Eppendof Centrifuge 5418). The spin column was rinsed with 400 µl 200 mM sodium phosphate buffer once. The concentrated NC probes were then recovered simply by placing the filter device upside down in a clean micro centrifuge tube and spin it at 1000 SPM for 2 minutes. The concentration of the NC probes after purification was characterized by NanoDrop spectrophotometer.

Before introducing the NC probes to the *MiSeq* chip, the purified NC probe sample was diluted to 500 nM using 200 mM sodium phosphate buffer. To hybridize the NC probes with the activator probes on *MiSeq* chip, 20 µl of 500 nM NC probe solution was injected into the chip using a pipette. The chip was heated to and maintained at 37 °C for 40 minutes. In our experiment, all fiducial markers (PhiX sequences) were stained with a common Atto488-labeled probe.

2.4 Library sequences design on the Illumina MiSeq chip

As mentioned above, the 18-nt long guanine-rich activator sequence was divided into 3 regions (6 nt for each region) and only one region was randomized at a time. Consequently, each region gave 4,096 sequence variations and 3 regions gave 12,288 variations in total. By tuning the density of reads on *MiSeq* chip, we ended up having ~250 duplicate polonies of each unique sequence (± 115 s.d.). About 52,000 duplicate polonies of the gold standard G15 sequence were also introduced to the chip and they served as a reference. For comparison, the full length of the activator probes was 170 nt long, which included not only the activator sequence but also the adaptors, primers and other sequences that Illumina used to facilitate sequencing.

2.5 Image acquisition and CHAMP alignment

A commercial software, Micro-Manager, was used to capture images from a Hammamatsu CMOS camera (ORCA-Flash 4.0). An auto-stage (Prior Scientific, OptiScan III), an auto-shutter (Shutter Instrument, Lambda SC) and a home-made control program were used to achieve automatic imaging acquisition. In this experiment, two image acquisition methods were used for C55. One was to acquire each field of view (FOV) for 1 s exposure time, and the other was to record the photobleaching behavior by acquiring each FOV for 30 ms exposure time and 300 images. The 1 s exposure time was by far the most appropriate condition for NCB imaging. Whereas shorter exposure time speeded up data acquisition, lower signal-to-noise ratio (SNR) was obtained. With similar idea, we applied Cy5 channel (EX/EM: 620/60, 700/75) to acquire C55 image simply because the SNR was the best. It is worthwhile to note that C55 is a bright fluorophore which can be seen throughout different fluorescence channel (i.e. Cy3, Cy 5.5, etc.). Apart from that, we used 1 s exposure time in FITC/Atto488 channel to acquire the PhiX images which served as reference fluorophores for the image alignment.

The image alignment of the *MiSeq* chip using the Chip-Hybridized Associated Mapping Platform (CHAMP) program (6) provided us a method to extract the sequence location information. The program has four main steps: *map*, *init*, *h5* and *align*. Starting from extracting the sequence information from fastq files provided by Illumina machine in the *map* command, the program generates a set of files which contains all interesting target sequences. Followed by the *h5* that combine all images into one single hdf5 file, the *init* sets the metadata for the condition (e.g. rotation angle, target names, etc.) to align. As to the last step, *align* transforms the sequence information in fastq files into pseudo-images. By applying cross-correlation, we will be able to register the raw PhiX images and extract the sequence information of that FOV. The results files contain not only the PhiX but also our library sequence information. Based on the results files, we can then link the intensity information with our library sequence and perform data analysis further.

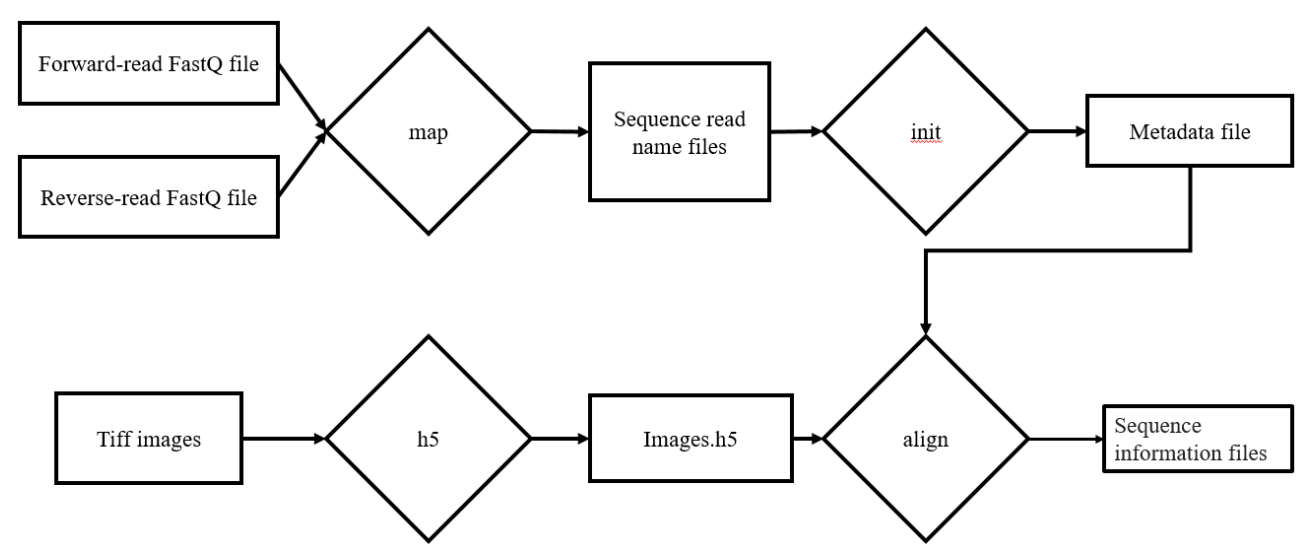


Figure 3. The simplified workflow of CHAMP alignment method. First of all, we applied *map* command to generate the correct sequence read name files. Secondly, we created the metadata file by using *init* command. Thirdly, we combined all tiff images (e.g. PhiX images) into hdf5 file by *h5* command for further processing. Lastly, the program would evaluate the position of each FOV by the condition recorded in the metadata file and extracted the sequence information from the sequence read name files with *align* command.

2.6 Assessment of intensity

To characterize the intensity ranking, we first split our 1024 by 1024 raw images to 512 by 512 subimages. Sequences associated with any errors or defects during Illumina sequencing process were discarded. For the data analysis, we emphasized on the statistics about fluorescence stability and intensity ranking. Because of the vignette illumination of epifluorescent microscope, we performed post-processing to correct our images. Along the correction within each FOV, we corrected the unequal illumination throughout the whole image batch. We collected the median value among all pixels and enhanced or reduced every pixel within every FOV by multiplying the ratio of the median value of each image to the median value of all median intensity. To collect the representative intensity for each single cluster, we applied normalized Gaussian to perform element-wise multiplication and summed all weighted intensity value within 7 by 7 area. After linking intensity information with sequences, we applied bootstrap method by repeatedly calculating the mean and standard deviation of 70% of each sequence 1000 times and applied the overall mean intensity and standard deviation to represent the intensity results. The ranking was based on the mean intensity after bootstrap calculation.

2.7 Assessment of intensity decay

To characterize the decay rates, we acquired the image by reducing the exposure time to 30 ms and recording 9 s for each FOV. Using similar idea, we applied Gaussian 2D kernel to collect the intensity information of each cluster throughout the image stack of each FOV. Since the exposure time in this experiment was short, and the uneven illumination situation was not severe, we did not apply vignette correction here. To keep the analysis simple, we fitted the intensity data with single exponential decay. Afterward, we directly applied bootstrap to compute the decay rate of each sequence. Since the actual value of each fluorophore might vary, we emphasized on the intensity change between the starting time point and 4.5 s.

2.8 Validation of intensity ranking

Since the synthesis yields, buffer conditions, and hybridization conditions can slightly vary from one batch to another, we have seen fluctuations in our brightness and photostability ranking in the repeated experiments. Therefore, we focused on the sequences which gave a stable ranking number among repeated experiments. To validate the ranking results, we selected 10 candidates which is 48 nt long containing 7 top-ranking sequences and 3 bottom-ranking sequences to compare with golden standard. Furthermore, to mimic the condition on the chip, we picked 4 sequences and extend them to 90 nt long. By hybridizing C55 Ag NCs (120 μ l) with activator candidates (1.5 μ l, 1.2 mM) separately, we then used

spectrometer (Hariba FluoroMax-4) to perform a 3D spectrum scanning. Since Cy5 channel was applied to perform image acquisition, the correlation evaluation between chip results and spectrometer results was made by analyzing the fluorescent intensity area within the channel excitation and emission range.

2.9 Validation of intensity decay ranking

To validate the intensity decay ranking using CHAMP and to evaluate whether there was correlation between intensity ranking and photostability, we hybridized C55 Ag NCs (120 μ l) with previously selected 10 activator candidates (1.5 μ l, 1.2 mM) separately, and recorded droplet (1 μ l) fluorescence decay behavior with the same excitation intensity. Since the concentration of fluorophores within a droplet was much higher than that on the chip, we reduced the exposure time to 30 ms and record 300 images for each kind of solution. The in-solution decay behavior was analyzed by computing intensity decrement of single pixel. Apart from that, because of the saturation, we evaluated the decay only after specific time point until the last frame.

3. RESULTS

3.1 Selection based on NCB brightness

From our CHAMP selection platform, we ranked all 12,288 sequences (from the brightest, 1, to the dimmest, 12,288) and found our gold standard G15 activator ranked 367. We selected 7 sequences from the top 50 candidates and tested one by one using the traditional in-solution preparation and fluorometer measurement method. Excitation and emission spectrum of the 10 selected activator sequences were measured using a Hariba FluoroMax-4 spectrometer. The 2D spectrums of the 48 nt long candidates are shown in Fig. 4. The sequence read name and the corresponding photon counts in Cy5 channel are listed in Table 1. Out of 7 bright candidates (48 nt), 4 of them confirmed our expectation. Interestingly, the brightest sequences in Cy5 channel is ranking 8, but not ranking 2 with highest peak intensity. On the other hand, we were able to predict correctly for the sequences which were not beneficial to the fluorescence increment as shown in both Table 1 and Fig. 4 for sequences ranking 10658, 10879 and 12103. The false positive results might result from the ignorance of extended bases of full-length sequences synthesized on the chip which we will evaluate the effect as our future work. Noted that the ranking for the sequence was based on a result of the first batch of experiment, only served for differentiating the trend without any other purposes.

NGS-based Brightness ranking	Sequence read names	Fluorometer reading (a.u.)	Results
2 (48 nt)	GAA TGG GGT GGG GTG GGG	96574040	True positive
3 (48 nt)	GGG TTT GGT GGG GTG GGG	48430980	False positive
4 (48 nt)	GTG GTG GGT GGG GTG GGG	30571790	False positive
8 (48 nt)	GGG TGG GGT GGG GAT GGC	323789120	True positive
15 (48 nt)	GGG TGG TCC GGT GTG GGG	31615950	False positive
25 (48 nt)	AGT GGT GGG GTG GGG	71115610	True positive
43 (48 nt)	ATG GGT GGG GTG GGG	74246100	True positive
Standard (rank 367, 48 nt)	GGG TGG GGT GGG GTG GGG	56558350	-
10658 (48 nt)	GAT TTC GGT GGG GTG GGG	36024440	True negative
10789 (48 nt)	TAT TCG GGT GGG GTG GGG	15313500	True negative
12103 (48 nt)	TAT TCA GGT GGG GTG GGG	11526740	True negative

Table 1. The list of all candidate sequences examined in the in-solution preparation and fluorometer measurement method. Here we only integrated the fluorescence emission within Cy5 excitation (590 - 650 nm) and emission (665 - 735 nm) range. Since the modification only happened in the changeable region, we only listed the changeable part for the 48 nt long sequences. The most promising activator sequence, rank 8, is highlighted in yellow.

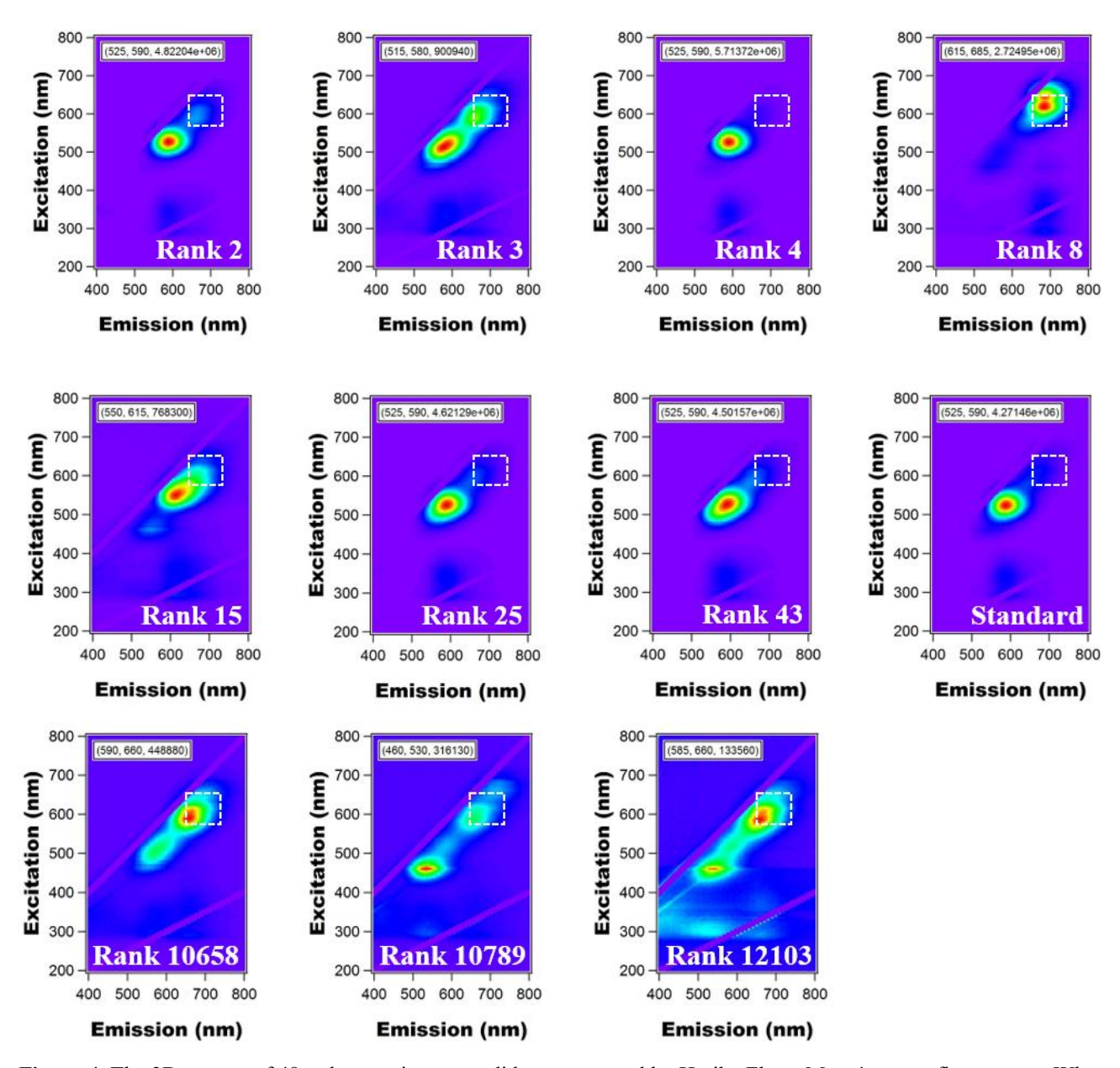


Figure 4. The 2D spectra of 48 nt long activator candidates measured by Hariba FluoroMax-4 spectrofluorometer. When compared with the standard (G15), these spectra gave 4 true positive, 3 false positive and 3 true negative results. The region for Cy5 excitation and emission was marked by a dashed box.

3.2 Selection based on NCB photostability

The activator sequences with the corresponding decay constant examined in solution and on the chip are listed in Table 2. We mainly examined the 48 nt long activator sequences. To validate the decay ranking results, we fitted the intensity in solution with single exponential decay ($y = a \times e^{-bx} + c$) as shown in Fig. 5. We defined the reciprocal of decay constant, b, in the exponential decay function as "ensemble decay time constant" to keep convention. To our surprise, although the prediction based on short exposure time does not match the in-solution results, the decay constant shows a tendency: large decay time constant for the top-ranking sequences (maximum: 8.33 s) comparing to small decay time constant for the bottom-ranking sequences (minimum: 3.11 s). Such consistency confirms the feasibility of NCB

photostability selection using CHAMP. On the other hand, comparing the decay constant of Atto647 with candidates in solution, we did find some activator sequences which were more photostable than Atto647.

NGS-based Brightness ranking	Sequence read names	Ensemble decay time constant in solution (s)	Predicting ranking number of photostability	Results
2 (48 nt)	GAA TGG GGT GGG GTG GGG	7.03	7804	False positive
3 (48 nt)	GGG TTT GGT GGG GTG GGG	4.62	5754	True positive
4 (48 nt)	GTG GTG GGT GGG GTG GGG	4.01	1091	True positive
8 (48 nt)	GGG TGG GGT GGG GAT GGC	7.77	225	True positive
15 (48 nt)	GGG TGG TCC GGT GTG GGG	8.33	3668	True positive
25 (48 nt)	AGT GGT GGT GGG GTG GGG	3.71	9086	True negative
43 (48 nt)	ATG GGT GGT GGG GTG GGG	4.31	4929	True positive
Standard (rank 367, 48 nt)	GGG TGG GGT GGG GTG GGG	3.92	6800	-
10658 (48 nt)	GAT TTC GGT GGG GTG GGG	3.81	3354	False positive
10789 (48 nt)	TAT TCG GGT GGG GTG GGG	4.26	4885	True positive
12103 (48 nt)	TAT TCA GGT GGG GTG GGG	3.11	11270	True negative
Atto647	-	4.13	-	-

Table 2. The in-solution decay validation results. The photostability selection performed much better than the brightness selection, giving more true positive results. The conclusion in *Results* was based on photostability ranking on the chip and the sequence ranking is followed the naming rules in Table 1. The most promising activator sequence, rank 15, is highlighted in yellow.

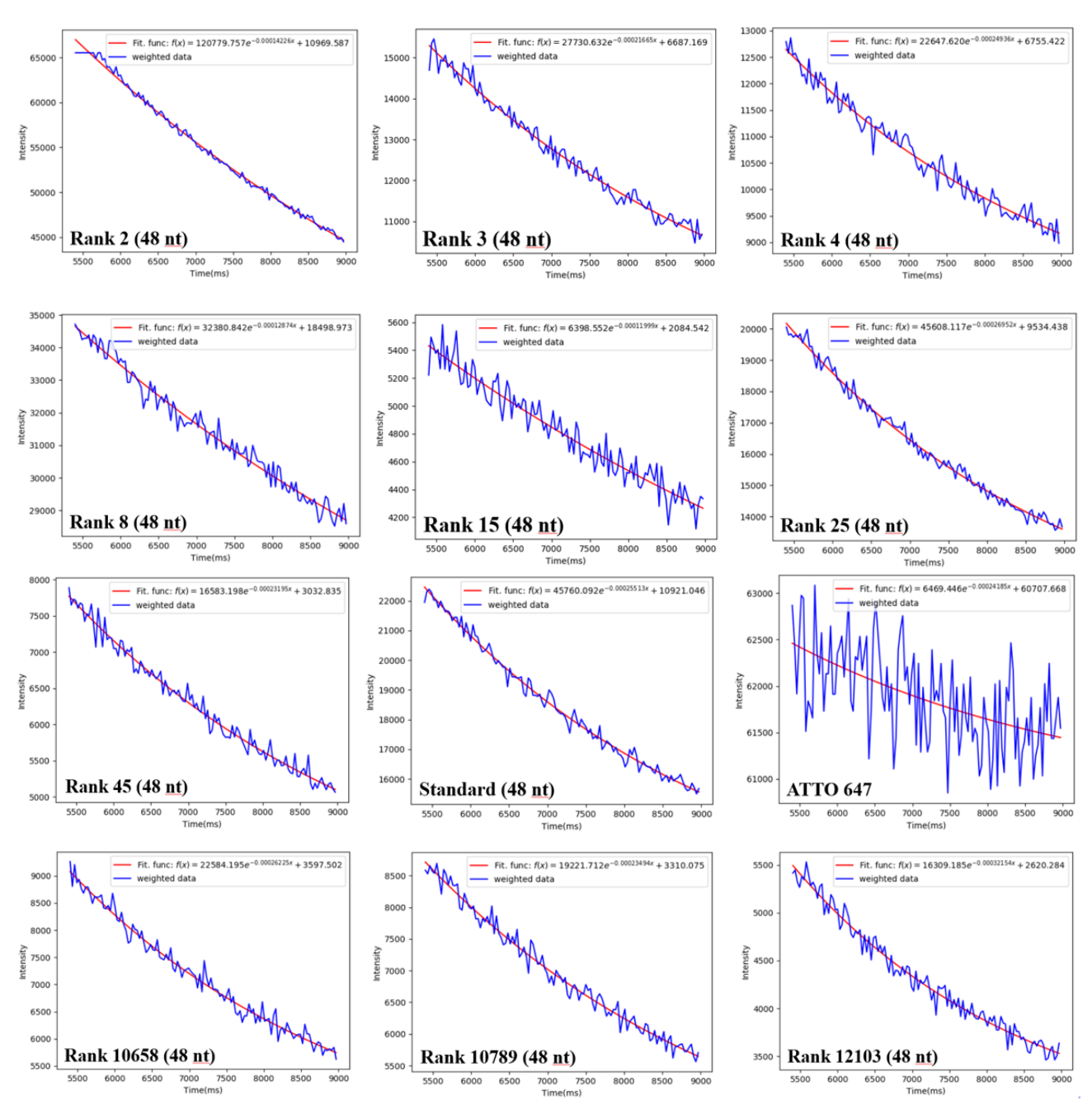


Figure 5. The in-solution decay fitting curves. Among these activator candidates, rank 15 was the most photostable, showing 8.33 s decay time constant, which is substantially longer than the time constant of Atto647 (4.13 s).

3.3 Alignment results visualization

We have developed an ImageJ plugin to facilitate the visualization of our alignment results. Simply put the raw images and the corresponding alignment results into one folder and select that folder. The plugin will combine all the images in the folder into a stack and associate the results files to the stack. By clicking on the canvas, we will be able to extract the sequence information stated in the **Materials and Methods 2.10**. Simplified examples are shown in Fig. 6 where we first click on a spot having fluorescence signal (marked in green) and then investigate the results having no fluorescence

(marked in blue). As our expectation, the panel presents the sequence information of the first position and showing *no sequence* for the second one.

Sequence name	Row	Col	Intensity info	Ranking
AGGGACGGTGGGGTGGGG	438.0	338.0	3496.14061522	7394
No Sequence	430.0	342.0	1869	No Ranking

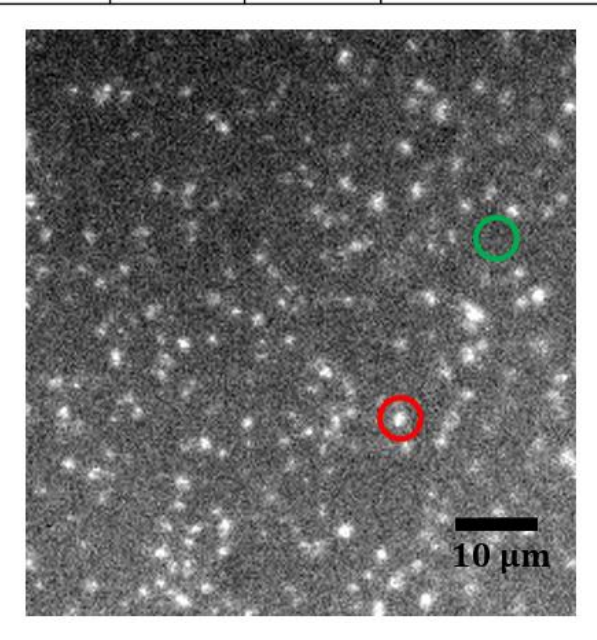


Figure 6. We have developed an ImageJ plugin to facilitate the visualization of our alignment results. The first click locating on the spot marked in green circle showed a promising activator candidate. The second click locating on the spot where no cluster was correctly presented the corresponding result. Noted that herein we only demonstrated the most important information rather than the full message stated in the **Materials and Methods 2.10**.

4. DISCUSSION

Attributed to the complexity of silver NCB formation, the theory of color tuning is still under debate. Gwinn group applied computational methods (e.g. support vector machine and motif mining) and gave a statistical insight to conquer the similar dilemma in different kinds of AgNCs cluster-nucleation sequence (5, 18). Albeit limited by the number of kinds of samples, their methodology paves the way for other scientists to search for the favorable sequences for metal cluster formation.

During the experiment, we discovered the ranking variance of sequences from batch to batch and hence we intentionally selected the sequences which were more stable among repeated experiments to evaluate our selection results. The inconsistency of intensity ranking but similar decay behavior between in-solution and on the chip experiments suggest the role of fluorescence decay in determining the intensity ranking. Within 1 s exposure, the fluorophores decay behavior will affect the overall intensity recorded in the image. Consequently, the intensity ranking would have more failure prediction comparing to the decay result. Besides, as shown in the Fig. 4, the correlation between decay constants with the prediction of intensity ranking reflecting the possibility of interference from photostability in deciding the most promising activator sequences as well.

On the other hand, the 2D spectrums of extended activator sequence confirmed our selection in a red channel. For example, the excitation and emission peak of rank 15 sequence changed from 550 nm and 615 nm to 615 nm and 685 nm; however, the excitation and emission peak of dark sequence such as rank 10789 sequence did not change much. The foregoing result demonstrated the ability of CHAMP to preferentially select brighter sequences in a high throughput manner. In our experiment, we discovered 4 kinds of 48 nt long brighter sequences (e.g. rank 2, rank 8, rank 25, rank 43).

Some of them showed intensity increment in the Cy5 channel range (e.g. rank 2, rank 25, rank 43) and the rank 8 sequence even shift the spectrum to red region.

Using the same platform, we provided a new method to select the more photostable sequence after hybridization with Ag NCs. From Fig. 4 and Table 2, the selected sequences (decay time constant: $4.01 \text{ s} \sim 8.33 \text{ s}$) decay slower than standard NCB (decay time constant: 3.92 s). With high accuracy of decay prediction, CHAMP method paved a new path for NCB photostability selection.

5. CONCLUSION

In this work, we repurposed the next-generation sequencing chip to perform high-throughput selection of promising NCB activator sequences. Ultimately, we would like to create a large database to predict other promising sequences using simple equipment. Toward the goal, we aim to polish our selection algorithm so that the accuracy of selection is acceptable. So far, we have selected several candidates and evaluated them using the traditional in-solution preparation and fluorometer measurement method. While the CHAMP-based intensity selection has much room to improve, we still are able to find NCBs that are brighter and more photostable than the current design. By exploring a vast ligand composition space and observing the corresponding activation behaviors of silver clusters, we aim to elucidate the design rules of NCBs.

6. ACKNOWLEDGEMENTS

This research is financially supported by Robert A. Welch Foundation (F-1833 to H.-C. Y.), National Science Foundation (Grant 1611451), and Associate Professor Experimental (APX) collaborative research fund at UT Austin (to H.-C. Y.). Jeff Petty thanks the National Institutes of Health (1R15GM102818) and the National Science Foundation EPSCoR Program under NSF Award #OIA-1655740. Special thanks for Jessica Podnar who helped us processing NGS chip production in GSAF and solve problem encountered during library preparation.

REFERENCES

- 1. H. C. Yeh et al., "A DNA-silver nanocluster probe that fluoresces upon hybridization," *Nano Letters* **10**(8), 3106-3110 (2010).
- 2. H. C. Yeh et al., "A fluorescence light-up Ag nanocluster probe that discriminates single-nucleotide variants by emission color," *Journal of the American Chemical Society* **134**(28), 11550-11558 (2012).
- 3. Y. A. Chen et al., "NanoCluster Beacons Enable Detection of a Single N(6)-Methyladenine," *Journal of the American Chemical Society* **137**(33), 10476-10479 (2015).
- 4. C. I. Richards et al., "Oligonucleotide-stabilized Ag nanocluster fluorophores," *Journal of the American Chemical Society* **130**(15), 5038-5039 (2008).
- 5. S. M. Copp et al., "Base motif recognition and design of DNA templates for fluorescent silver clusters by machine learning," *Advanced Materials* **26**(33), 5839-5845 (2014).
- 6. C. Jung et al., "Massively Parallel Biophysical Analysis of CRISPR-Cas Complexes on Next Generation Sequencing Chips," *Cell* **170**(1), 35-47 (2017).
- 7. H. Kobayashi et al., "New strategies for fluorescent probe design in medical diagnostic imaging," *Chemical Reviews* **110**(5), 2620-2640 (2010).
- 8. J. T. Petty et al., "A Segregated, Partially Oxidized, and Compact Ag10 Cluster within an Encapsulating DNA Host," *Journal of the American Chemical Society* **138**(10), 3469-3477 (2016).
- 9. J. M. Obliosca, C. Liu, and H. C. Yeh, "Fluorescent silver nanoclusters as DNA probes," *Nanoscale* **5**(18), 8443-8461 (2013).
- 10. J. Zhang et al., "Hairpin DNA-Templated Silver Nanoclusters as Novel Beacons in Strand Displacement Amplification for MicroRNA Detection," *Analytical Chemistry* **88**(2), 1294-1302 (2016).
- 11. J. Sharma et al., "Silver nanocluster aptamers: in situ generation of intrinsically fluorescent recognition ligands for protein detection," *Chemical Communications* **47**(8), 2294-2296 (2011).
- 12. J. Li et al., "Binding-Induced Fluorescence Turn-On Assay Using Aptamer-Functionalized Silver Nanocluster DNA Probes," *Analytical Chemistry* **84**(12), 5170-5174 (2012).

- 13. J. Liu et al., "Label-free and fluorescence turn-on aptasensor for protein detection via target-induced silver nanoclusters formation," *Analytica Chimica Acta* **749**(70-74 (2012).
- 14. K. Zhang et al., "A label-free kissing complexes-induced fluorescence aptasensor using DNA-templated silver nanoclusters as a signal transducer," *Biosensors and Bioelectronics* **78**(154-159 (2016).
- 15. J. Yin et al., "Label-free and turn-on aptamer strategy for cancer cells detection based on a DNA-silver nanocluster fluorescence upon recognition-induced hybridization," *Analytical Chemistry* **85**(24), 12011-12019 (2013).
- 16. J. M. Obliosca et al., "A complementary palette of NanoCluster Beacons," ACS Nano 8(10), 10150-10160 (2014).
- 17. Y. A. Chen et al., "Improving NanoCluster Beacon performance by blocking the unlabeled NC probes," *Chemical Communications* **55**(4), 462-465 (2019).
- 18. S. M. Copp et al., "Fluorescence Color by Data-Driven Design of Genomic Silver Clusters," ACS Nano (2018).